Chance-Constrained Optimization in D2D-Based Vehicular Communication Network

Zhixin Liu, Yuan'ai Xie, Kit Yan Chan, Kai Ma, *Member, IEEE*, and Xinping Guan, *Fellow, IEEE*

***Abstract*—In this paper, a novel scheme is proposed to optimize the effectiveness of the device-to-device (D2D) enabled vehicular communications (D2D-V), which are underlaid in cellular networks, where the uplink channel allocated to one cellular user (CU) is reused by the multiple D2D-V links. To develop a well-functioning D2D-V system, the sum rate of all D2D-V links is necessary to be maximized, and also the reliability of the co-channel CU to infrastructure has to be guaranteed with the CU interference constraint. Unlike the traditional statical D2D systems, the D2D-V system suffers with high mobility and channel uncertainty. Therefore, the CU interference constraint is formulated as a probabilistic function by the Bernstein approximation, the constraint attempts to address the mobile channel fluctuations. Besides, the tractable approximate constraint is reformulated as two separable structure, this reformulated constraint attempts to determine the near-optimal solutions more efficiently. Since the objective function with a logarithmic form is nonconvex, successive convex approximation is applied to transform the nonconvex problem into the convex problem. The dual decomposition is used to determine the near-optimal solutions. After the problem is reformulated, a distributed robust power control algorithm is proposed to perform the chance-constrained optimization. Numerical simulations are used to evaluate the performance of the proposed scheme. The simulation results show the impacts of system performance when applying the proposed scheme in vehicular environments with high mobility. The proposed optimization schemes are further verified by comparing with the existing methods.**

***Index Terms*—Device-to-device (D2D) communication, power control, vehicular communications, channel uncertainty, chance-constrained programming.**

I. Introduction

TO REDUCE traffic congestion and improve traffic safety, effective vehicular communications are essential. In vehicular communications, an effective cooperation is generally required among vehicles in a close range. Vehicles are necessary to receive proper status information (e.g. real-time GPS, velocity, direction and perhaps, some emergency warnings) and other sharing infotainment data from their vicinities. Moreover, higher data transmission rates are required, since the information flow and data flow have to be large enough to exchange frequent status information and to perform vehicle-mounted multimedia services.

Previous solutions for vehicular communication are mostly the ad-hoc communications over the 802.11p standard and backend-based communications over the Long Term Evolution (LTE) cellular standard [1], [2]. However, there are some limitations in these communication modes. For the 802.11p system, as claimed in [3], the system is primarily optimized for a WLAN-type of environment when the mobility is zero or very low. Therefore, the vehicular ad-hoc network (VANET) is likely to be crashed by connectivity disruptions and signal congestions which are caused by rapid changing of network topology, particularly in peak-hour. Besides, the utilization rate of spectrum resources is low in pure ad-hoc topology [4]. As the number of access vehicles increases, broadcast storms occur more frequently. For the conventional cellular system, the traditional LTE is not able to sustain V2V communications natively since the packets have to be relayed by the Evolved Node B (eNB) [5], [6]. Compared with the direct communication between adjacent vehicles, this approach is inefficient since this approach causes higher latency and poor reliability. Thus, as the supplement of the centralized cellular architecture, proximity-based device-to-device (D2D) links are introduced since D2D underlay communication can provide direct local message dissemination with low latency and better reliability.

A. Related Works

D2D underlay communication, integrating the advantages of ad-hoc network and conventional LTE cellular network, is currently served as an essential solution for vehicular communication [1], [3], [7]. In D2D underlaying cellular networks, proximity users can directly communicate with each other without going through eNB. Unlike the traditional D2D networks with low mobility such as mobile smart phones, the device-to-device-enabled vehicular communications (D2D-V) terminals have the following characteristics. Firstly, due to the subordinate location relationship between adjacent vehicles, the D2D-V terminals no longer obey the two-dimensional Poisson

Manuscript received September 20, 2018; revised December 11, 2018 and January 27, 2019; accepted March 4, 2019. Date of publication March 11, 2019; date of current version May 28, 2019. This work was supported in part by the National Natural Science Foundation of China under Grant 61873223, Grant 61473247, and Grant 61571387 and in part by the Natural Science Foundation of Hebei Province under Grant F2017203140 and Grant F2017203084. The review of this paper was coordinated by Prof. P. Lorenz. *(Corresponding author: Zhixin Liu.)*

Z. Liu, Y. Xie, and K. Ma are with the Institute of Electrical Engineering, Yanshan University, Qinhuangdao 066004, China (e-mail: lzxauto@ysu.edu.cn; xieyuan_ai@163.com; kma@ysu.edu.cn).

K. Y. Chan is with the School of Electrical Engineering, Computing and Mathematical Sciences, Curtin University, Perth, WA 6845, Australia (e-mail: kit.chan@curtin.edu.au).

X. Guan is with the School of Electronic, Information and Electrical Engineering, Shanghai Jiaotong University, Shanghai 200240, China (e-mail: xpguan@sjtu.edu.cn).

This paper has supplementary downloadable material available at http://ieeexplore.ieee.org, provided by the authors.

Digital Object Identifier 10.1109/TVT.2019.2904291

Point Process. Hence more realistic traffic flow model, such as the constant speed motion model [8], [9] and Cowan's M3 model [10], [11] are considered. Secondly, since the vehicle mobility is high, the periodical renewed channel state information (CSI) and GPS message are adopted to assist the vehicles to accomplish the D2D-V grouping strategies and decentralized power control algorithms. Besides, there are two limitations in D2D-V system. On the one hand, most of previous works consider the configuration that any channel of cellular user (CU) is reused by at most one D2D link [12], [13]. However, the fact that multiple D2D-V links and the cellular link share the same channel matches the high vehicle density scenarios perfectly, and improves spectrum efficiency by higher number of D2D links [7], [14]. It may also decrease the system performance due to the mutual interference. On the other hand, the majority of the literatures assume that the eNB senses the global instantaneous CSI of all the D2D and cellular links, but this assumption is not practical for the fast moving D2D-V system. Motivated by these two principal limitations, a robust power control scheme by using the interference management strategy and considering the uncertainty of CSI should be developed to maximize the sum rate of all D2D-V links and guarantee the quality of service (QoS) of CU. To tackle the first limitation in D2D-V system, the existing methods have been developed based on the interference management schemes [15]–[18]. In [15], the power control scheme is proposed based on Geometric Programming, in order to tackle these nonlinear optimization problems which are involved with a system-wide objective (e.g., maximizing the total system throughput) and the QoS constraints. The scheme also attempts to ensure the interference limits. In [16], an efficient power control iterative algorithm is developed to maximize the achievable sum rate of the underlying cognitive radio microcellular system and control the interference between the macrocell and the microcell with a satisfaction level. The communication problem is attempted to optimize the network sum rate of the secondary users and is constrained with the inferences of the primary users. The problem is solved by the beamformers and the iterative dual subgradient (IDuSuG) algorithm in [17]. Ren *et al.* [18] proposed a simplified power control framework to maximize the sum rate or the minimal achievable rate of the D2D-V system. Almost all of the previously developed approaches attempt to maximize the network sum rate which is subject to the interference constraints in the underlay scenario. The original objective function of power control is nonlinear (neither convex nor concave) function to the transmit powers. These optimization problems can be simplified or converted into a convex problem which can be solved by the convex optimization theory. Unlike the simplified sum rate maximization problem in [18], the successive convex approximation (SCA) method is applied to transform the nonconvex problem into the convex one by setting a series of concave lower bounds on the objective function [15]–[17]. The computational complexity of optimizing the transformed problem is low. Therefore, the SCA method is commonly used to solve the sum rate maximization problem which is subject to the interference constraints in underlay network.

All aforementioned power control schemes require the assumption that the actual CSI are available. However, it is impractical, since the channel uncertainty and quantization errors exist in real situations, especially in high-mobility vehicular environments. In addition to the impractical assumption, the optimization with instantaneous CSI requires a real-time power control scheme where the computational complexity is high and the communication overhead is generated. The users are likely to experience poor performance, since the power control scheme is deployed with an impractical assumption. Hence, to overcome the second limitation in D2D-V system, it's necessary to address the uncertainties when the power control scheme is deployed. However, the CU interference constraint is nonstationary since the channel is changing. The CU interference constraint can be modeled as a chance constraint which is more difficult to tackle than the deterministic counterparts. Chance constraints are mostly nonconvex and it is difficult to express them in closed form [19]. To obtain the closed form, Nemirovski and Shapiro have proposed a convex approximation approach of chance constraints in [20]. Thereinto, Bernstein method has commonly been used to approximate the probabilistic constraint with channel uncertainty [21]–[24]. In addition, the instantaneous sum rate cannot be acquired since the uncertainties of CSI exist. Therefore, the long term rate is used to replace the instantaneous achievable rate in larger time scales [25]. In the D2D-V communication network, vehicle locations are time-varying due to the high mobility. Hence, this is unlikely that the feedback of the CSIs can be accurately captured from the vehicles. For lower communication overhead, the sampling feedback of the CSIs is captured periodically by a receiver. Therefore, the long term rate is also applicable in our proposed method.

B. Contribution

In this paper, we formulated a robust power control problem which is involved with the multi-user interference and the imperfect CSI in the D2D-based underlay vehicular network. Unlike the existing papers which are subject to one or two previously mentioned limitations, our paper breaks through these two limitations at one stroke and proposes effective robust power control schemes. The key contributions of this paper are summarized as follows:

- For the first limitation, the more reasonable D2D application scenarios where multiple D2D-V links and one cellular link share the same channel are considered. To tackle the non-convex sum rate maximization objective involving with the multi-user interference, the SCA method with the low computational complexity is adopted and the nonconvex objective is transformed into the convex one.
- For the second limitation, the high channel uncertainty of dynamic vehicular network is considered, and a mobile channel model based on first-order Gauss-Markov process is adopted to describe the impacts of the Doppler frequency shift on the channel. To obtain the closed form of the chance constraint involving with CSI uncertainty, the Bernstein method is used. Since the error gain of the channel model is exponentially distributed, the mechanism of the Bernstein method is redeveloped to satisfy these conditions. Also, this is the first time to deploy the rigorous analysis to obtain the relevant safe approximation parameters.

TABLE I
NOTATIONS

$\Pr\{\cdot\}$	Probability function
$\mathbb{R}^n$	Set of n-dimensional real vectors
$\mathbb{E}\{\cdot\}$	Mathematical expectation of a random variable
$\mathbb{D}\{\cdot\}$	Variance of a random variable
$E\{\cdot\}$	Exponential distribution
Υ	Parameter of exponential distribution
$\boldsymbol{a}^T$	Transpose of vector $\boldsymbol{a}$
$\mathcal{N}$	The index set of orthogonal channels $\mathcal{N}$=$\{1, 2, \cdots, N\}$
$\mathcal{M}$	The index set of reused channels $\mathcal{M}$=$\{1, 2, \cdots, M\}$
$\mathcal{K}$	The index set of D2D-V transmitters $\mathcal{K}$=$\{1, 2, \cdots, K\}$
$\mathcal{J}$	The index set of receivers $\mathcal{J}$=$\{0, 1, \cdots, K\}$

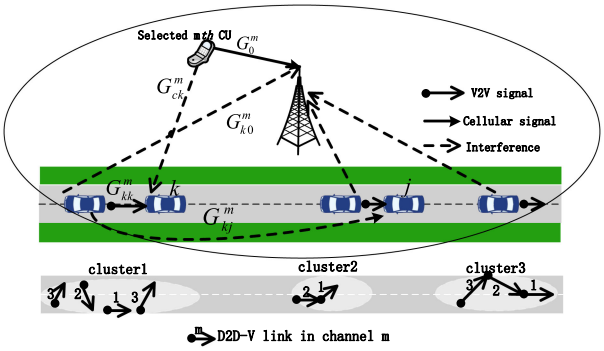

Fig. 1. System model.

- To pursue an efficient solution, the constraint with multiple coupled variables which is transformed by Bernstein method is further reformulated into two constraints with tractable separable structures, where the reformulated constraints are more feasible to be treated. The distributed algorithm is developed to solve the optimization problem which is involved with the reformulated constraints. To determine the error channel gain which can be involved with a bounded or unbounded support, a procedure is proposed to resolve the channel uncertainty.

The rest of the paper is organized as follows: Section II presents the system and channel models, as well as the problem formulation. In Section III, the original problem which is non-convex is transformed into the convex one by the SCA and Bernstein methods. The distributed power control iterative algorithm is developed in Section IV. Simulation results and performance analysis are presented in Section V. Finally, the conclusions are drawn in Section VI.

Notation: In this paper, vectors are typefaced using bold lowercase letters. Some notations are given in Table I.

II. Problem Definition

A. System and Channel Models

In this paper, a D2D-enabled vehicular communication network is involved in a single cell with radius R, as depicted in Fig. 1. The eNB lies on the cell center and one straight unidirectional highway passes through its coverage region. The distance from the eNB to the highway is denoted as D, and the length of the highway inside the cell coverage is given as $d = 2\sqrt{R^2 - D^2}$. Numerous clusters are on the cell-covered section. The clusters are spontaneously formed when the distance between two neighbor vehicles exceeds the applicable distance of D2D communication. Cowan's M3 model stated that the distances between adjacent clusters follow a truncate exponential distribution. Hence, vehicle speeds are assumed to satisfy the constant speed motion model when a small time interval is considered. Both single or multiple neighbor vehicle pairs are in each cluster. Although the distance between each neighbor vehicle pair is normally small, the distance usually satisfies the minimum safety requirement. More specifically, all vehicles are duplex and each of them is equipped with a transmit antenna and a receive antenna. In order to avoid the self interference between the duplex communication, the transmit and receive antennas on a vehicle are assumed to be operating at different channels, the transmit or receive antennas of any two neighbor vehicles are matched as a pair and share the same channel. The remaining two antennas are matched with the other adjacent vehicles by occupying two extra channels. Each adjacent vehicle pair conducts direct D2D communication by reusing the uplink channel of a cellular user (CU). However, the two proximal vehicles from different clusters transmit information at dedicated channels [7], through the eNB. Therefore, when N orthogonal uplink channels are supposed to be allocated to the wayside CU, M ($M \leq N$) channels are reused by D2D-V links. In the real communication environment, the number of vehicles is larger than the number of reusable uplink channels. Hence, multiple vehicles share the same uplink channel. To minimize the mutual interference, Ren *et al.* [18] proposed a round channel selection fashion. In this approach, the eNB is required to divide all the D2D-V links into M individual groups which are corresponding to the M reused channels. When a D2D-V link enters the investigated cell from another cell, it needs to be registered to the eNB, and one of the M group indexes is required to be assigned. For example, supposing the link is indexed with i, and the group index mod$\{i, M\}$ $+ 1$ is assigned to this vehicle. When the next D2D-V link comes within this coverage region, the link is indexed with $i + 1$ and is assigned with the group index, (mod$\{i + 1, M\} + 1$). Therefore, the D2D-V links are assigned to different groups. Fig. 1 illustrates the D2D-V grouping strategy with case of $M = 3$.

The D2D-V system consists of four kinds of communication links, namely CU-I link, V2I link, V2V link and CU-V link. Two types of channel models are generally used to address these four kinds of communication links. Specifically, the first type of channel models is used to describe the communication links with no mobility (i.e. CU-I link), and the second type of these channel models is dedicated to the communication links with high mobility (i.e. V2I link, V2V link and CU-V link).

Channel Model I: CU-I link: The channel power gain of CU-I link, G_0^n, between the stationary CU in the nth channel and the eNB is given as:

$$G_0^n = L_0^n |h_0^n|^2, n \in \mathcal{N} \tag{1}$$

where L_0^n denotes the large-scale fading effects including shadow-fading and path loss, and h_0^n denotes the small-scale fast fading component which is assumed to be independent and

identically distributed $(i.i.d.)$ in $\mathcal{CN}(0,1)$ [26]. Therefore, the small-scale fast fading $\psi_0^n = |h_0^n|^2$ is an exponential random variable with the parameter $\Upsilon = 1$, which is given as

$$\psi_0^n \sim E(1). \tag{2}$$

Proof: See Appendix A ■

Channel Model II: V2I link, D2D-V link and CU-V link: Since the vehicle mobility is generally fast, it is difficult to estimate the accurate CSIs for the other mobile links which are connected with the vehicles. To estimate a more accurate mobile channel gain, the CSI of V2I link is assumed to be reported to the eNB periodically with a period of T_0, and the CSIs of V2V link and CU-V link are broadcasted to the vehicle with a period of T_1 $(T_1 < T_0)$. The first-order Gauss-Markov process [26], [27] is adopted to model the channel fluctuation (fast fading) with the period,

$$h = \epsilon \hat{h} + e, \tag{3}$$

where h and $\hat{h}$ denote the channel responses of the mobile links in the previous and current time respectively. The coefficient ϵ $(0 \le \epsilon < 1)$ quantifies the channel correlation between the two consecutive time slots, e is the channel discrepancy term which is with the distribution of $\mathcal{CN}(0, 1-\epsilon^2)$ and is independent to $\hat{h}$. In Kim *et al.*'s statistical model [27], ϵ is formulated by $\epsilon = J_0(2\pi f_D T)$, where $J_0(\cdot)$ is the zero-order Bessel function. $f_D = \upsilon f_c / c$ is the maximum Doppler frequency with $c = 3 \times 10^8$ m/s. f_c is the carrier frequency, and υ represents the vehicle speed. T is the variable which denotes the CSI feedback time interval. In detail, the earlier T_0 and T_1 are the specific constant values of T.

For the V2I and V2V links, the channel power gain model is given as a unified expression:

$$G_{kj}^m = L_{kj}^m((\epsilon_{kj}^m \hat{h}_{kj}^m)^2 + |e_{kj}^m|^2), j \in \mathcal{J}, k \in \mathcal{K}, m \in \mathcal{M}. \tag{4}$$

where L_{kj}^m denotes the large-scale fading effects including shadow-fading and path loss from kth transmitter to jth receiver in channel m. (4) consists of the large-scale fading L_{kj}^m and the small-scale fast fading component (3), which is similar to (1).

Given that $\hat{g}_{kj}^m = L_{kj}^m(\epsilon_{kj}^m \hat{h}_{kj}^m)^2$, and $\tilde{g}_{kj}^m = L_{kj}^m |e_{kj}^m|^2$, (4) can be reformulated as,

$$G_{kj}^m = \hat{g}_{kj}^m + \tilde{g}_{kj}^m, \qquad j \in \mathcal{J}, k \in \mathcal{K}, m \in \mathcal{M}, \tag{5}$$

where G_{k0}^m denotes the V2I link's channel gain from the kth D2D-V transmitter of the mth group to the eNB when $j = 0$; G_{kj}^m is the V2V link's channel gain from the kth D2D-V transmitter to jth D2D-V receiver in mth group when $j \neq 0$ and $j \neq k$; G_{kk}^m is the effective channel gain of the kth D2D-V link in the mth group when $j = k$; Moreover, $\hat{g}_{kj}^m$ and $\tilde{g}_{kj}^m$ are the sampling channel gains in previous time and error channel gain among these mobile channels respectively. $\hat{g}_{kj}^m$ is the measuring constant. $\tilde{g}_{kj}^m$ is an exponential random variable which is given by $\tilde{g}_{kj}^m \sim E(\frac{1}{L_{kj}^m \sqrt{1-\epsilon_{kj}^{m\,2}}})$.[1]

[1]The parameter transformation is proved by Appendix B.

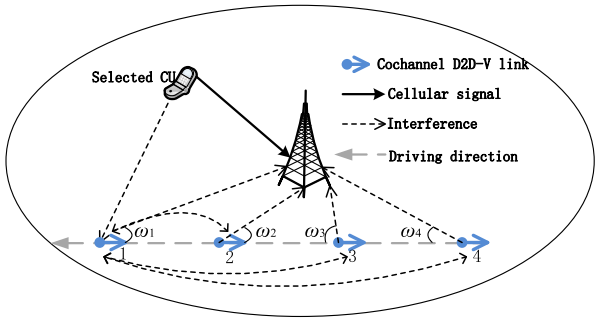

Fig. 2. Simplified system model ($K = 4$).

For the CU-V link, the interference channel gain from the mth CU to the kth D2D-V link namely, G_{ck}^m, can be similarly estimated by (3) with the vehicle sampling period, T_1.

The SINR at the eNB from the mth $(m \in \mathcal{M})$ CU with the reused channel is defined as,

$$\gamma_0^m = \frac{p_0^m G_0^m}{\sum_{k=1}^K p_k^m G_{k0}^m + \delta^2}, \tag{6}$$

the SINR at kth D2D-V link on the mth channel is,

$$\gamma_k^m = \frac{p_k^m G_{kk}^m}{\sum_{j=1, j\neq k}^K p_j^m G_{jk}^m + p_c^m G_{ck}^m + \delta^2} \tag{7}$$

respectively, where p_c^m and p_k^m denote the transmit powers of the mth CU and the kth D2D-V transmitter in mth channel respectively. δ^2 is the noise power. Especially, the transmit powers of the CUs can be determined and are uncontrollable. Hence, p_c^m is considered as a constant.

B. Problem Formulation

When the D2D underlay communication is incorporated with the communication architecture of the system, the SINR requirement on the CU has to be satisfied. Hence, the transmitter power constraint of the D2D-V links has to be satisfied too. To maximize the D2D-V system performance, both the SINR and the transmitter powers have to be optimized to achieve a relatively high level and a sufficiently high rate. This can be achieved by an effective power control scheme. Since the M uplink reused channels are mutually orthogonal, no interchannel interference exists in the whole single-cell cellular network. Hence, the performance of the whole system can be optimized on a single channel. In vehicular communication scenario, this is infeasible to obtain an accurate global CSI. When the previous channel gain statistical models are combined, the relevant robust power control strategy is proposed to optimize the D2D-V system performance.

Fig. 2 shows a simplified system model of which the K D2D-V links reuse one CU's uplink channel. The figure also shows that the D2D-V links are indexed from 1 to K. Based on (7), the SINR namely $\gamma_k(\mathbf{p})$ at the kth $(k \in \mathcal{K})$ D2D-V link in the reused channel can be formulated as,

$$\gamma_k(\mathbf{p}) = \frac{p_k G_{kk}}{\sum_{j=1, j\neq k}^K p_j G_{jk} + p_c G_{ck} + \delta^2}, \tag{8}$$

where p_k denotes the transmit power of kth D2D-V links, and $\mathbf{p} \triangleq [p_1, p_2, \ldots, p_K]$ is the power vector.

However, the real-time SINR is impractical to be captured in the vehicular communication system since the channel gain is time-varying and the computational cost is high. One can only measure the long-term SINR in a very small time interval by using the channel estimation techniques which use the shared status informations for the vehicles. When the simplified scenario is used, the real-time SINR is replaced with the long-term SINR since the CSI feedback time interval is very small. Therefore, to maximize the long term sum rate [25] of all the K D2D-V links with the CU interference probabilistic constraint, a robust optimization problem is formulated as follows:

$$\begin{aligned} &\max_{\mathbf{p}} W \sum_{k=1}^{K} \log_2(1+\bar{\gamma}_k(\mathbf{p})) \\ &\text{s.t.} \begin{cases} \Pr\left\{\sum_{k=1}^{K} G_{k0} p_k \le I_{th}\right\} \ge 1-\varepsilon \\ 0 \le p_k \le p_{k,\max} \end{cases} \end{aligned} \tag{9}$$

where W is the bandwidth of a reused channel; $\bar{\gamma}_k(\mathbf{p})$ denotes the long-term SINR of the kth D2D-V link when a short CSI feedback time interval is used; $p_{k,\max}$ is the maximum power of kth D2D-V transmitter; I_{th} is the eNB threshold of the tolerable interference; and the constraint attempts to ensure that the aggregated interference caused by all the K D2D-V links should be smaller than I_{th}.

III. Transformations of the Nonconvex Problem

In this section, the nonconvex original problem in (9) is transformed into a standard concave maximization problem by Bernstein and SCA methods. Two approximate interference constraints with separate structures are further determined by exploiting appropriate bounds, which attempt to determine the near-optimal solutions. In particular, two cases of error channel gain with bounded or unbounded support are proposed, and these two error channel gains are optimized separately to satisfy the conditions by using Bernstein method.

A. Approximation of Probability Constraint

To tackle the intractability of the probability constraint in (9), a convex approximation method namely Bernstein approximations [20], [19] is proposed. The probability constraint (10) is formulated as,

$$\Pr\left\{ f_0(\mathbf{p}) + \sum_{n=1}^{N} \eta_n f_n(\mathbf{p}) \le 0 \right\} \ge 1-\varepsilon, \tag{10}$$

where $\mathbf{p}$ is a deterministic parameter vector, and $\{\eta_n\}$ are the random variables with the marginal distributions, $\{\xi_n\}$. Suppose that one desires to satisfy the constraint (10) for a given family of $\{\eta_n\}$ distributions, when the following conditions are assumed:

1) $\{f_n(\mathbf{p})\}$ is affine in $\mathbf{p}$;
2) $\{\eta_n\}$ is independent of each other;
3) $\{\xi_n\}$ has a common bounded support of $[-1, 1]$, which is in the range of $-1 \le \xi_n \le 1, \forall n = 1, 2, \ldots, N$.

The following constraint constitutes a substitute of conservative approximation,

$$\inf_{\rho>0} \left[f_0(\mathbf{p}) + \rho \sum_{n=1}^{N} \Omega_n(\rho^{-1} f_n(\mathbf{p})) + \rho \ln\left(\frac{1}{\varepsilon}\right) \right] \le 0, \tag{11}$$

where $\Omega_n(y) = \max_{\xi_n} \ln(\int \exp(xy) d\xi_n(x))$. Since (11) is convex [19], [20], (11) can be used to solve (9) if $\Omega_n(y)$ can be efficiently calculated. In general, the calculation can be performed by the upper bound of $\Omega_n(y)$ which is given by

$$\Omega_n(y) \le \max\{\mu_n^- y, \mu_n^+ y\} + \frac{\sigma_n^2}{2} y^2, n = 1, \ldots, N, \tag{12}$$

where μ_n^-, μ_n^+ with $-1 \le \mu_n^- \le \mu_n^+ \le 1$, and $\sigma_n \ge 0$ are the constants which can be determined by the given families of the probability distributions. Some examples are given in Table I of [19], but the parameters of the exponential distribution are not given in the table. The approximation is more complicated when more prior knowledge is required. Therefore, the expectations and the variances are only calculated to determine the relevant safe approximation parameters for the random variables of the exponential distribution. Appendix C shows how the values of μ^-, μ^+ and σ are obtained.

When $\Omega_n(\cdot)$ in (11) is substituted with this upper bound and the arithmetic-geometric inequality, a convex conservative surrogate for (10) can be formulated as (13),

$$\begin{aligned} f_0(\mathbf{p}) + \sum_{n=1}^{N} \max\{\mu_n^- f_n(\mathbf{p}), \mu_n^+ f_n(\mathbf{p})\} \\ + \sqrt{2\ln\left(\frac{1}{\varepsilon}\right)} \left(\sum_{n=1}^{N} \sigma_n^2 f_n(\mathbf{p})^2 \right)^{\frac{1}{2}} \le 0, \end{aligned} \tag{13}$$

Here the distributions of $\tilde{g}_{k0}$ are assumed to be bounded by $[a_k, b_k]$, and the unbounded supports will be discussed in the following subsection. The constants $\alpha_k = \frac{1}{2}(b_k - a_k) \ne 0$ and $\beta_k = \frac{1}{2}(b_k + a_k)$ are used to normalize the supports within the range of $[-1, 1]$, where the supports are given as

$$\xi_k = \frac{\tilde{g}_{k0} - \beta_k}{\alpha_k} \in [-1, 1]. \tag{14}$$

Given that $f_0(\mathbf{p}) = -I_{th} + \sum_{k=1}^{K} (\hat{g}_{k0} + \beta_k) p_k$ and $f_k(\mathbf{p}) = \alpha_k p_k$ for $k \in \mathcal{K}$, (10) is equivalent to the probability constraint in (9). Hence, substituting $f_0(\mathbf{p})$ and $f_k(\mathbf{p})$ into (13), the constraint can be reformulated as,

$$\begin{aligned} -I_{th} + \sum_{k=1}^{K} (\hat{g}_{k0} + \beta_k) p_k + \sum_{k=1}^{K} \mu_k^+ \alpha_k p_k \\ + \sqrt{2\ln\left(\frac{1}{\varepsilon}\right)} \left(\sum_{k=1}^{K} (\sigma_k \alpha_k p_k)^2 \right)^{\frac{1}{2}} \le 0. \end{aligned} \tag{15}$$

In the last term of (15), the variables p_k are coupled nonlinearly. Hence, the computational complexity of determining the optimal $\mathbf{p}$ increases rapidly when K increases. To reduce the computational complexity, the dual decomposition method is used. This method is applicable to solve the problem with

a separable structure. After the constraint is reformulated in Lagrange form, smaller computational effort is only required to solve this optimization problem. To formulate a separable structure, the last term in (15) containing ℓ_2-norm of the vector $[\sigma_1\alpha_1 p_1, \ldots, \sigma_K\alpha_K p_K]$ is further approximated by $\|\mathbf{x}\|_2 \leq \sqrt{K}\|\mathbf{x}\|_\infty$ for any $\mathbf{x} \in \mathbb{R}^K$. Hence, (15) is reformulated as

$$\sum_{k=1}^{K} \chi_k p_k + \sqrt{2K \ln\left(\frac{1}{\varepsilon}\right)} \max_{k\in\mathcal{K}} \sigma_k \alpha_k p_k \leq I_{th}, \tag{16}$$

where $\chi_k = \hat{g}_{k0} + \mu_k^+ \alpha_k + \beta_k$.

Alternatively, the fact that $\|\mathbf{x}\|_2 \leq \|\mathbf{x}\|_1$ can be used to acquire another alternative of (9) as

$$\sum_{k=1}^{K} \chi_k p_k + \sqrt{2\ln\left(\tfrac{1}{\varepsilon}\right)} \sum_{k=1}^{K} |\sigma_k \alpha_k p_k| \leq I_{th}. \tag{17}$$

Therefore, (9) can be dubbed as the ℓ_2-, ℓ_∞-, and ℓ_1-approximate problems, when the probabilistic constraint is replaced by (15), (16) and (17) respectively.

Although the corresponding probabilistic constraint is non-convex or hard to extract closed-form approximations, it may be rational to apply Bernstein approximation if the three conditions including boundedness of the support of the distribution are all satisfied. The following subsection discusses the error channel gain which is unbounded under the ideal environment.

B. Extension to Error Channel Gain With Unbounded Support

In the previous subsection, the Bernstein approximation is used to determine the bounded error channel gain. It is feasible to adopt the bounded error channel gain in the actual wireless communication system, but the more specific characteristic information for the uncertain parameters is likely to bring a looser approximation of the probabilistic constraint. Therefore, the error channel gain with unbounded support, $\tilde{g}_{k0}$, is necessary to be discussed.

Define $I \triangleq \sum_k G_{k0} p_k$. By substituting $G_{k0} = \hat{g}_{k0} + \tilde{g}_{k0}$, $\Pr\{I \leq I_{th}\}$ in (9) is reformulated as

$$\begin{aligned}\Pr\{I \leq I_{th}\} = \Pr\{I \leq I_{th} | \mathbf{a} \leq \tilde{\boldsymbol{g}} \leq \mathbf{b}\} \Pr\{\mathbf{a} \leq \tilde{\boldsymbol{g}} \leq \mathbf{b}\} \\ + \Pr\{I \leq I_{th} | \tilde{\boldsymbol{g}} \leq \mathbf{a} \text{ or } \tilde{\boldsymbol{g}} \geq \\ \mathbf{b}\} \Pr\{\tilde{\boldsymbol{g}} \leq \mathbf{a} \text{ or } \tilde{\boldsymbol{g}} \geq \mathbf{b}\},\end{aligned} \tag{18}$$

where $\tilde{\boldsymbol{g}} = [\tilde{g}_{10}, \ldots, \tilde{g}_{K0}]^T$, $\mathbf{a} = [a_1, \ldots, a_K]^T$ and $\mathbf{b} = [b_1, \ldots, b_K]^T$ are the appropriate constants. $\Pr\{\mathbf{a} \leq \tilde{\boldsymbol{g}} \leq \mathbf{b}\}$ can be further elaborated as,

$$\theta \triangleq \Pr\{\mathbf{a} \leq \tilde{\boldsymbol{g}} \leq \mathbf{b}\} \in (1-\varepsilon, 1). \tag{19}$$

Since the last term in (18) is smaller than $(1-\theta)$, disregarding this term, (9) can be conservatively approximated as

$$\Pr\{I \leq I_{th} | \mathbf{a} \leq \tilde{\boldsymbol{g}} \leq \mathbf{b}\} \approx \frac{\Pr\{I \leq I_{th}\}}{\Pr\{\mathbf{a} \leq \tilde{\boldsymbol{g}} \leq \mathbf{b}\}} \geq \frac{1-\varepsilon}{\theta} \triangleq 1 - \varepsilon', \tag{20}$$

which can be approximated by (16) or (17) and ε is replaced by ε'. When the ideal CSI feedback condition is assumed, $\tilde{g}_{k0}$ is an exponential random variable with an unbounded support. The probability density function of $\tilde{g}_{k0}$ is defined as (21),

$$f_{\tilde{g}_{k0}}(x) = \frac{1}{\bar{g}_{k0}} \exp\left(-\frac{x}{\bar{g}_{k0}}\right), \tag{21}$$

where the mean is $\bar{g}_{k0} = L_{k0}\sqrt{1-\epsilon_{k0}^2}$. Based on the independence assumption, $\Pr\{\mathbf{a} \leq \tilde{\boldsymbol{g}} \leq \mathbf{b}\}$ can be elaborated as,

$$\begin{aligned}\Pr\{\mathbf{a} \leq \tilde{\boldsymbol{g}} \leq \mathbf{b}\} &= \prod_{k=1}^{K} \Pr\{a_k \leq \tilde{g}_{k0} \leq b_k\} \\ &= \prod_{k=1}^{K} \left[\exp\left(-\frac{a_k}{\bar{g}_{k0}}\right) - \exp\left(-\frac{b_k}{\bar{g}_{k0}}\right)\right] = \theta.\end{aligned} \tag{22}$$

Since the crest value of the $p.d.f.$ of $\tilde{g}_{k0}$ is at the origin, the lower-bound can be chosen as $\mathbf{a} = \mathbf{0}$. To determine $\mathbf{b}$, $\Pr\{0 \leq \tilde{g}_{k0} \leq b_k\}$ is set to a constant value for all V2I links. Hence, $\mathbf{b}$ is calculated by

$$b_k = \bar{g}_{k0} \ln \frac{1}{1-\theta^{\frac{1}{N}}}. \tag{23}$$

Based on the Bernstein approximation, the probability constraint can be transformed into a deterministic convex constraint, when the channel gain is engaged either the bounded supports or unbounded supports. However, the objective function is a $d.c.$ functions which is dependent on the power vector $\mathbf{p}$. Since this problem is involved with the $d.c.$ structure, this is an NP-hard problem [28]. The global optimum in (9) is difficult to be determined. Therefore, the objective function is reformulated as a convex optimization problem by a successive approximation method which is discussed next.

C. Successive Convex Approximation of the Objective Function

Since the objective function in (9) cannot be converged at $\mathbf{p}$, (9) is reformulated as a convex optimization problem by the successive convex approximation. When the lower bound is used for the approximation, (24) can be used to compute the long term sum rate, R_{sum}, for all the K D2D-V links in the simplified system,

$$\begin{aligned}R_{sum} &= W \sum_{k=1}^{K} \log_2(1 + \bar{\gamma}_k(\mathbf{p})) \\ &\geq \frac{W}{\ln 2} \sum_{k=1}^{K} [A_k \ln(\bar{\gamma}_k(\mathbf{p})) + B_k] \triangleq R_{sum,lb},\end{aligned} \tag{24}$$

where A_k and B_k can be chosen as $A_k = \varsigma_k/(1+\varsigma_k)$ and $B_k = \ln(1+\varsigma_k) - A_k \ln(\varsigma_k)$, for any given $\varsigma_k > 0$ [29]. The equality in (24) is only valid when both $A_k = \bar{\gamma}_k(\mathbf{p})/(1+\bar{\gamma}_k(\mathbf{p}))$ and $B_k = \ln(1+\bar{\gamma}_k(\mathbf{p})) - A_k \ln(\bar{\gamma}_k(\mathbf{p}))$ are valid. (A_k, B_k) =(1,0) when $\bar{\gamma}_k(\mathbf{p})$ approaches the plus infinity.

Proof: See Appendix D ■

Consequently, the objective function in (9) can be approximated by setting the lower bound as follows:

$$\max_{\mathbf{p}} \frac{W}{\ln 2} \sum_{k=1}^{K} [A_k \ln(\bar{\gamma}_k(\mathbf{p})) + B_k]. \tag{25}$$

(25) is still a non-convex problem since the objective function is not convex with respect to the vector $\mathbf{p}$. However, when the transformation $\tilde{p}_k = \ln p_k$ is used, a set of standard concave maximization problem can be transformed in term of the new variables $\tilde{p}_k$ in ℓ_1- and ℓ_∞-approximate problems. Papandriopoulos and Evans [29] have proved that the substituted objective function with the deterministic constraint is a standard concave maximization problem, since $\tilde{p}_k$ are the decoupled variables.

IV. Distributed Power Control Algorithm

The power control problem, which maximizes the long term sum rate, has the separable structure. The optimization of this power control problem can be performed by optimizing each variable in $\tilde{\mathbf{p}} = [\tilde{p}_1, \ldots, \tilde{p}_K]$. The ℓ_1-approximate problem is clearly separable in $\tilde{\mathbf{p}}$. For the ℓ_∞-approximate problem, (16) can be reformulated as the separable constraints (26) and (27), by introducing auxiliary variables $\boldsymbol{\nu} \triangleq [\nu_1, \ldots, \nu_K]$ [21],

$$\sum_{k=1}^{K} \chi_k \mathrm{e}^{\tilde{p}_k} + \sqrt{2\ln\left(\frac{1}{\varepsilon}\right)} \sum_{k=1}^{K} \nu_k \le I_{th}, \tag{26}$$

$$\sqrt{K}\sigma_k \alpha_k \mathrm{e}^{\tilde{p}_k} \le \sum_{k'=1}^{K} \nu_{k'}, \qquad k \in \mathcal{K}. \tag{27}$$

The power control algorithm is developed by incorporating with (26) and (27). The ℓ_1-approximation is briefly discussed in Section IV-B.

A. Iterative Algorithm for the ℓ_∞-Approximation

Based on the separable constraints and the objective function given in (26), (27) and (25), the robust optimization problem in (9) can be reformulated as

$$\max_{\tilde{\mathbf{p}}} \frac{W}{\ln 2} \sum_{k=1}^{K} \left[A_k \ln(\bar{\gamma}_k(\mathrm{e}^{\tilde{\mathbf{p}}})) + B_k\right]$$
$$\text{s.t.} \begin{cases} \sum_{k=1}^{K} \chi_k \mathrm{e}^{\tilde{p}_k} + \sqrt{2\ln\left(\frac{1}{\varepsilon}\right)} \sum_{k=1}^{K} \nu_k \le I_{th} \\ \sqrt{K}\sigma_k \alpha_k \mathrm{e}^{\tilde{p}_k} \le \sum_{k'=1}^{K} \nu_{k'}, \qquad k \in \mathcal{K} \\ -\infty \le \tilde{p}_k \le \ln p_{k,\max}, \qquad k \in \mathcal{K} \end{cases} \tag{28}$$

When the dual variables $\mu \ge 0$ and $\boldsymbol{\lambda} \triangleq [\lambda_1, \ldots, \lambda_K]^T \ge 0$ are integrated into (26) and (27), respectively, the convex problem can be solved by Lagrange dual decomposition technique [30]. The Lagrangian of (28) is formulated as,

$$L(\tilde{\mathbf{p}}, \boldsymbol{\nu} : \mu, \boldsymbol{\lambda}) = \frac{W}{\ln 2} \sum_{k=1}^{K} \left[A_k \ln(\bar{\gamma}_k(\mathrm{e}^{\tilde{\mathbf{p}}})) + B_k\right]$$
$$- \mu \left(\sum_{k=1}^{K} \chi_k \mathrm{e}^{\tilde{p}_k} + \sqrt{2\ln\left(\frac{1}{\varepsilon}\right)} \sum_{k=1}^{K} \nu_k - I_{th} \right)$$
$$- \sum_{k=1}^{K} \lambda_k \left(\sqrt{K}\sigma_k \alpha_k \mathrm{e}^{\tilde{p}_k} - \sum_{k'=1}^{K} \nu_{k'} \right). \tag{29}$$

Hence, the corresponding dual function is given as,

$$\begin{aligned} D(\mu, \boldsymbol{\lambda}) &= \max_{-\infty \le \tilde{p}_k \le \ln p_{k,\max}} L(\tilde{\mathbf{p}}, \boldsymbol{\nu} : \mu, \boldsymbol{\lambda}) \\ &= \max_{-\infty \le \tilde{p}_k \le \ln p_{k,\max}} \sum_{k=1}^{K} \left\{ \frac{W}{\ln 2} \left[A_k \ln(\bar{\gamma}_k(\mathrm{e}^{\tilde{\mathbf{p}}})) + B_k\right] \right. \\ &\quad - \left(\mu\chi_k + \lambda_k \sqrt{K}\sigma_k\alpha_k\right) \mathrm{e}^{\tilde{p}_k} \\ &\quad \left. + \left(\sum_{k'=1}^{K} \lambda_{k'} - \mu\sqrt{2\ln\left(\frac{1}{\varepsilon}\right)} \right) \nu_k \right\} + \mu I_{th}, \end{aligned} \tag{30}$$

where $\mu = (-2\ln\varepsilon)^{-\frac{1}{2}} \sum_{k'=1}^{K} \lambda_{k'}$. The dual problem can be reformulated as

$$\min_{\boldsymbol{\lambda} \succeq \mathbf{0}, \mu \ge 0} D(\mu, \boldsymbol{\lambda}). \tag{31}$$

Here, the sub-gradient method is used to update $\boldsymbol{\lambda}$ and the procedure is depicted as follows:

$$\lambda_k^{(t+1)} = \left[\lambda_k^{(t)} + \phi_k \left(\sqrt{K}\sigma_k\alpha_k \mathrm{e}^{\tilde{p}_k} + \frac{\sum_{k=1}^{K} \chi_k \mathrm{e}^{\tilde{p}_k} - I_{th}}{\sqrt{-2\ln\varepsilon}}\right)\right]^+, \tag{32}$$

where $[x]^+ = \max[0, x]$, $\phi_k > 0$ denotes the diminishing step-size and t denotes the iteration index.

Maximization of the inner dual function, $D(\mu, \boldsymbol{\lambda})$, can be performed by determining the stationary point of (27) with respect to $\boldsymbol{\lambda}$ and $\tilde{\mathbf{p}}$:

$$\frac{\partial L(\tilde{\mathbf{p}}, \boldsymbol{\nu} : \mu, \boldsymbol{\lambda})}{\partial \tilde{p}_k} = \frac{W}{\ln 2} A_k - \left(\frac{W}{\ln 2} \sum_{j \ne k}^{K} A_j \frac{\bar{\gamma}_j(\mathrm{e}^{\tilde{\mathbf{p}}}) \overline{G_{kj}}}{\mathrm{e}^{\tilde{p}_j} \overline{G_{jj}}} + \mu\chi_k + \lambda_k\sqrt{K}\sigma_k\alpha_k \right) \mathrm{e}^{\tilde{p}_k} = 0, \tag{33}$$

where $\overline{G_{jk}}$ and $\overline{G_{jj}}$ are the expectation values of G_{jk} and G_{jj} respectively; $\overline{G_{jk}} = \mathbb{E}\{G_{jk}\} = \hat{g}_{jk} + \bar{g}_{jk}$ with $\mathbb{E}\{\hat{g}_{jk}\} = \hat{g}_{jk}$ and $\mathbb{E}\{\tilde{g}_{jk}\} = \bar{g}_{jk}$; $\overline{G_{jj}} = \mathbb{E}\{G_{jj}\} = \hat{g}_{jj} + \bar{g}_{jj}$ with $\mathbb{E}\{\hat{g}_{jj}\} = \hat{g}_{jj}$ and $\mathbb{E}\{\tilde{g}_{jj}\} = \bar{g}_{jj}$. Moreover, $\bar{\gamma}_j(\mathrm{e}^{\tilde{\mathbf{p}}})$ denotes the long term SINR of the jth D2D-V link and is given by

$$\bar{\gamma}_j(\mathrm{e}^{\tilde{\mathbf{p}}}) = \frac{\mathrm{e}^{\tilde{p}_j}\overline{G_{jj}}}{\sum_{k=1,k\ne j}^{K} \mathrm{e}^{\tilde{p}_k}\overline{G_{kj}} + p_c\overline{G_{cj}} + \delta^2}. \tag{34}$$

Based on (33), the iteration for the power allocation , $\tilde{\mathbf{p}}^{(t+1)}$, can be formulated as,

$$\tilde{p}_k^{(t+1)} = \left[\ln\left(\frac{W A_k^{(t)}}{\ln 2}\right) - \ln\left(\frac{W}{\ln 2} \sum_{j \ne k}^{K} A_j^{(t)} \frac{\bar{\gamma}_j^{(t)}(\mathrm{e}^{\tilde{\mathbf{p}}}) \overline{G_{kj}}}{p_j^{(t)} \overline{G_{jj}}} + \mu^{(t)}\chi_k + \lambda_k^{(t)}\sqrt{K}\sigma_k\alpha_k \right) \right]_{-\infty}^{\ln p_{k,\max}}, \tag{35}$$

where $[x]_a^b = \min\{\max\{x, a\}, b\}$, $\mu^{(t)} = \frac{\sum_{k=1}^{K} \lambda_k^{(t)}}{\sqrt{-2\ln\varepsilon}}$, and $A_k^{(t)} = \bar{\gamma}_k^{(t)}(\mathrm{e}^{\tilde{\mathbf{p}}})/(1 + \bar{\gamma}_k^{(t)}(\mathrm{e}^{\tilde{\mathbf{p}}}))$. The power iteration in (35) is distributed through a combination of measurement and message-passing [29]. The convergence can be proved by the standard interference function in [31]. The distributed robust power control algorithm is developed based on the successive convex approximation (SCA) method which is discussed in the following subsection.

Algorithm 1: Distributed Robust Power Control Algorithm Based on the SCA Method.

Set the maximum number of iterations $I_{\max}$ and the step size ϕ;
Initialize the iteration counter $t \leftarrow 1$, $\tilde{\mathbf{p}} \leftarrow \tilde{\mathbf{p}}_0$;
Initialize $\boldsymbol{\lambda}$ for the ℓ_∞-approximation. [Alternatively, set μ for the ℓ_1-approximation].
repeat
Calculate $\bar{\gamma}_k^{(t)}(\mathrm{e}^{\tilde{\mathbf{p}}})$ for $\forall k \in \mathcal{K}$
$A_k^{(t)} \leftarrow \bar{\gamma}_k^{(t)}(\mathrm{e}^{\tilde{\mathbf{p}}})/(1+\bar{\gamma}_k^{(t)}(\mathrm{e}^{\tilde{\mathbf{p}}}))$ and
$B_k^{(t)} \leftarrow \ln(1+\bar{\gamma}_k^{(t)}(\mathrm{e}^{\tilde{\mathbf{p}}})) - A_k^{(t)}\ln(\bar{\gamma}_k^{(t)}(\mathrm{e}^{\tilde{\mathbf{p}}}))$
Update $\tilde{\mathbf{p}}$ using (35). [Alternatively, update $\tilde{\mathbf{p}}$ using (37)].
Update $\boldsymbol{\lambda}$ using (32), $\mu^{(t)} \leftarrow \frac{\sum_{k=1}^{K}\lambda_k^{(t)}}{\sqrt{-2\ln\varepsilon}}$. [Alternatively, update μ using (38)].
$t \leftarrow t+1$.
until $\tilde{\mathbf{p}}$ and $\boldsymbol{\lambda}$ converge synchronously to the optimal solution $\tilde{\mathbf{p}}^*$ and $\boldsymbol{\lambda}^*$ or $t > I_{\max}$
[Alternatively, $\tilde{\mathbf{p}}$ and μ converge to the optimal solution $\tilde{\mathbf{p}}^*$ and μ^* or $t > I_{\max}$].

B. Iterative Algorithm for the ℓ_1-Approximation

The ℓ_1-approximate problem is solved similarly by the dual method. When the lagrangian multiplier $\mu \geq 0$ is integrated into (17), the iteration function for the transformed power vector $\tilde{\mathbf{p}}$ can be determined as

$$\frac{\partial L(\tilde{\mathbf{p}}:\mu)}{\partial \tilde{p}_k} = \frac{W}{\ln 2}A_k - \left(\frac{W}{\ln 2}\sum_{j\neq k}^{K} A_j \frac{\bar{\gamma}_j\left(\mathrm{e}^{\tilde{\mathbf{p}}}\right)\overline{G_{kj}}}{\mathrm{e}^{\tilde{p}_j}\overline{G_{jj}}} + \mu\left(\chi_k + \sqrt{2\ln\left(\frac{1}{\varepsilon}\right)}|\sigma_k\alpha_k|\right)\right)\mathrm{e}^{\tilde{p}_k} = 0, \tag{36}$$

and for $\forall k \in \mathcal{K}$,

$$\tilde{p}_k^{(t+1)} = \left[\ln\left(\frac{WA_k^{(t)}}{\ln 2}\right) - \ln\left(\frac{W}{\ln 2}\sum_{j\neq k}^{K} A_j^{(t)} \frac{\bar{\gamma}_j^{(t)}\left(\mathrm{e}^{\tilde{\mathbf{p}}}\right)\overline{G_{kj}}}{p_j^{(t)}\overline{G_{jj}}} + \mu^{(t)}\left(\chi_k + \sqrt{2\ln\left(\frac{1}{\varepsilon}\right)}|\sigma_k\alpha_k|\right)\right)\right]_{-\infty}^{\ln p_{k,\max}}. \tag{37}$$

The lagrangian multiplier μ can also be updated by using the sub-gradient method, and the procedure is described as follows:

$$\mu^{(t+1)} = \left[\mu^{(t)} + \phi\left(\sum_{k=1}^{K}\chi_k\mathrm{e}^{\tilde{p}_k} + \sqrt{2\ln\left(\frac{1}{\varepsilon}\right)}\sum_{k=1}^{K}|\sigma_k\alpha_k|\mathrm{e}^{\tilde{p}_k} - I_{th}\right)\right]^{+}. \tag{38}$$

TABLE II
SYSTEM PARAMETERS

Parameter	Value
Carrier frequency (f_c)	2 GHz
Cell radius (R)	500 m
Distance from highway to eNB (D)	10 m
Sampling period of eNB (T_0)	0.5 ms
Sampling period of vehicle (T_1)	0.1 ms
Average speed of vehicle	30 m/s
Bandwidth (W)	10 MHz
Mean of background noise (δ^2)	-30 dBm
Maximum D2D-V power ($p_{k,max}$)	0.05W

TABLE III
CHANNEL MODELS FOR V2I AND V2V LINKS [26]

Parameter	V2V and V2I links
Pathloss model	$128.1 + 37.6\log_{10} d$, d in km
Shadowing disturibution	Log-normal
Shadowing standard deviation	3 dB
Fast fading	Rayleigh fading

TABLE IV
RELATIVE VELOCITY $|\Delta V|$ FOR V2I AND V2V LINKS

Item	$\lvert\Delta\mathbf{V}\rvert$ ($\mathbf{T}^2$ / $\mathbf{R}^1$)	D_1 (32m/s)	D_2 (30m/s)	D_3 (34m/s)	D_4 (34m/s)	D_5 (30m/s)
V2V	D_1'(32m/s)	0m/s	2m/s	2m/s	2m/s	2m/s
	D_2'(30m/s)	2m/s	0m/s	4m/s	4m/s	0m/s
	D_3'(34m/s)	2m/s	4m/s	0m/s	0m/s	4m/s
	D_4'(34m/s)	2m/s	4m/s	0m/s	0m/s	4m/s
	D_5'(30m/s)	2m/s	0m/s	4m/s	4m/s	0m/s
V2I	eNB(0m/s)	31.06m/s	11.96m/s	9.91m/s	15.48m/s	25.55m/s

[1] $\mathbf{T}$:Transmitter.
[2] $\mathbf{R}$: Receiver.

V. SIMULATION RESULTS AND PERFORMANCE ANALYSIS

In this section, the numerical simulations are performed to evaluate the performance of the proposed Algorithms 1. The scenario is the simplified D2D-V system which consists of five co-channel D2D-V pairs. The major system parameters are given in Table II and the parameters for the channel models are given in Table III. It's noted that the carrier frequency f_c and the bandwidth W are set as 2 GHz and 10 MHz respectively in the numerical simulations, and the impact of other physical parameters are neglected. If other carrier frequency or bandwidth parameters are selected, the impacts of the neglected physical parameters such as thermal noise should be considered. Specially, the traffic flow of the highway is simulated as the Cowan's M3 model [11], where two adjacent vehicles in the same cluster are required to establish D2D-V link. Besides, the vehicle velocities are assumed to be a constant for a small time interval [9]. The velocities of the five co-channel D2D-V pairs are given in Table IV, and the values of θ and I_{th} are set as $1-0.5\varepsilon$ and 10^{-4} respectively. Since the impact of Doppler shift on the channel is considered, the relative velocities of all V2V and V2I links are calculated and are given in Table IV. Unlike the V2V links, the links and vehicle directions of the V2I are not collinear. Thus, the relative velocities of V2I links are obtained by multiplying the cosine of the intersection angle[2] between the V2I links and the vehicle directions [32].

[2]The intersection angles are illustrated by ω_1, ω_2, ω_3 and ω_4 in Fig. 2, respectively.

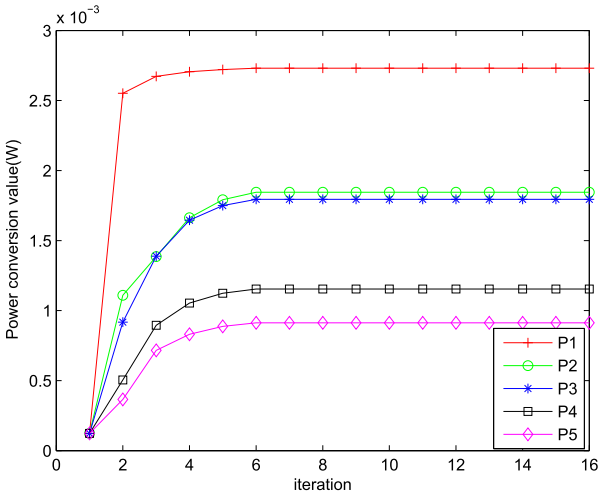

(a) ℓ_1-approximation algorithm with bounded CSI

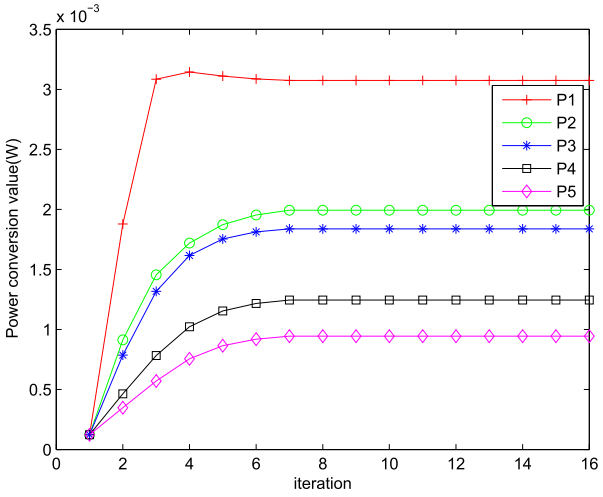

(b) ℓ_∞-approximation algorithm with bounded CSI

Fig. 3. Power convergence performance with bounded CSI.

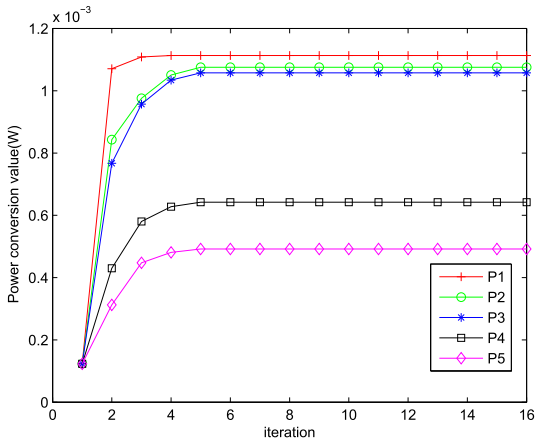

(a) ℓ_1-approximation algorithm with unbounded CSI

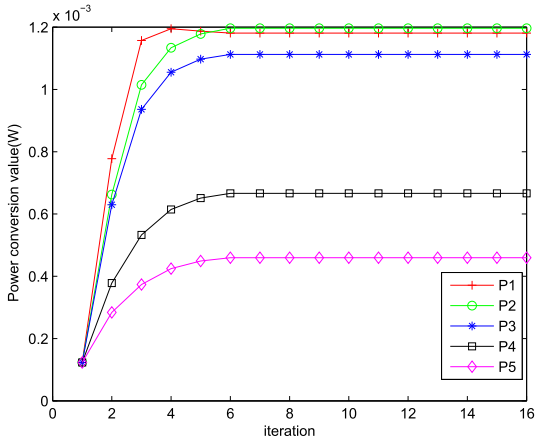

(b) ℓ_∞-approximation algorithm with unbounded CSI

Fig. 4. Power convergence performance with unbounded CSI.

Figs. 3 and 4 illustrate the transmission power of the five D2D-V transmitters with the bounded and unbounded CSI, respectively. Fig. 3 depicts that the power of each D2D-V transmitter can converge to the equilibriums. The legend entries with P1-P5 are also shown in the figure. The results in Fig. 3 show that all the cases of bounded CSI can be converged when Algorithm 1 is used. Moreover, Fig. 3(a) shows all powers can be converged after 6 iterations when the ℓ_1-approximation algorithm is used. Fig. 3(b) shows all powers can be converged after 7 iterations when the ℓ_∞-approximation algorithm is used. Fig. 4 shows the convergence of the five D2D-V transmitters' powers when the unbounded CSI is considered. Fig. 4(a) shows all powers can be converged after 5 iterations when the ℓ_1-approximation algorithm is used, Fig. 4(b) shows all powers can be converged after 6 iterations when the ℓ_∞-approximation algorithm is used. Comparing with the convergence results of the Fig. 3(a) and Fig. 3(b), Fig. 4(a) and Fig. 4(b) show that the lower convergence values and faster convergence rates can be achieved by Algorithm 1 when the unbounded CSI is considered. These four figures show that the ℓ_1-approximation algorithm has quicker convergence rates than those of the ℓ_∞-approximation algorithm.

To further demonstrate the performance of the proposed method, Fig. 5 depicts the long term sum rates when different values of ε are used. The solid line with lower triangulars correspond to the case that the CSIs of the V2V and V2I links are perfectly known. In this case, the probabilistic constraint in (9) comes down to a deterministic interference constraint. Hence, the long term sum rates are independent to ε. The results of the other cases show that the long term sum rates increase when ε increases, since greater ε generates a looser chance constraint. Therefore, the algorithm of ℓ_1-approximation is capable to achieve a slightly better performance than that of the algorithm of ℓ_∞-approximation. For the Bernstein approximation-based algorithms, the cases of bounded CSI yield better performances than the cases of unbounded CSI since the wider fluctuating ranges of CSIs render more confined ranges of transmit powers. These results show that the channel uncertainty has a significant impact on the system performance.

For the case of unbounded CSI, Fig. 6 shows the sensitivity of the long term sum rate performance when different θ and different outage probabilities (either $\varepsilon = 0.1$ or $\varepsilon = 0.3$) are used.

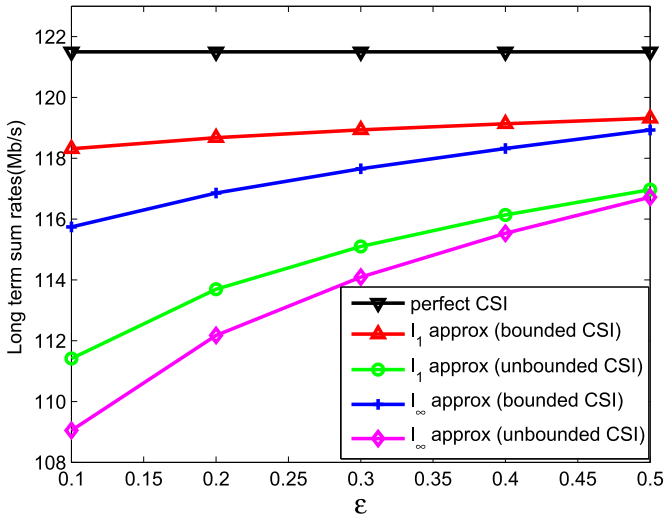

Fig. 5. Long term sum rates using in different cases.

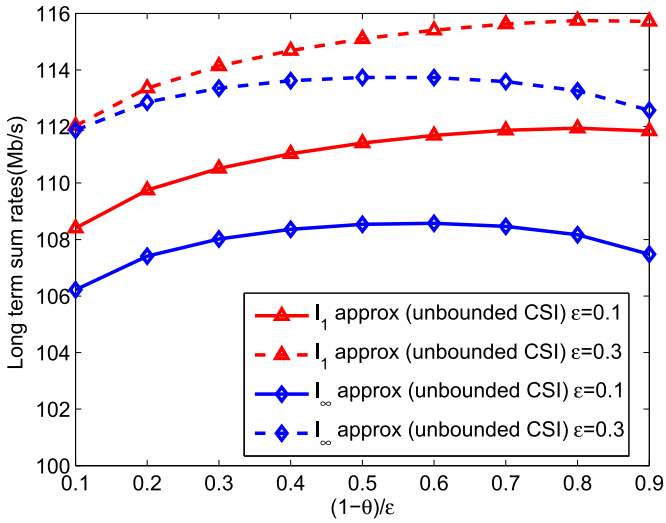

Fig. 6. Long term sum rates versus θ .

The figure shows that the performance of ℓ_1-approximation is maximized when $\theta = 1-0.5\varepsilon$ and this is robust when different θ is used. However, the performance of ℓ_∞-approximation is maximized when $\theta = 1-0.8\varepsilon$ and the robustness is relatively poorer comparing to the ℓ_1-approximation. Similar characteristics can be found when a different outage probability ε is used.

Fig. 7 shows the long term sum rates of the Bernstein approximation-based algorithms when different interference threshold, I_{th}, is used. Aforementioned, the aggregate interference caused by D2D-V links in one channel is required to be less than I_{th} in most cases. Apparently, the increased I_{th} can improve the performances of the D2D-V links when the same outage probability is used, since higher transmit powers achieve successful message transmission. Fig. 7 shows that the performances of the Bernstein approximation-based algorithms increase when I_{th} increases. Moreover, comparing with the case of unbounded CSI, the long term sum rates are higher in that of bounded CSI.

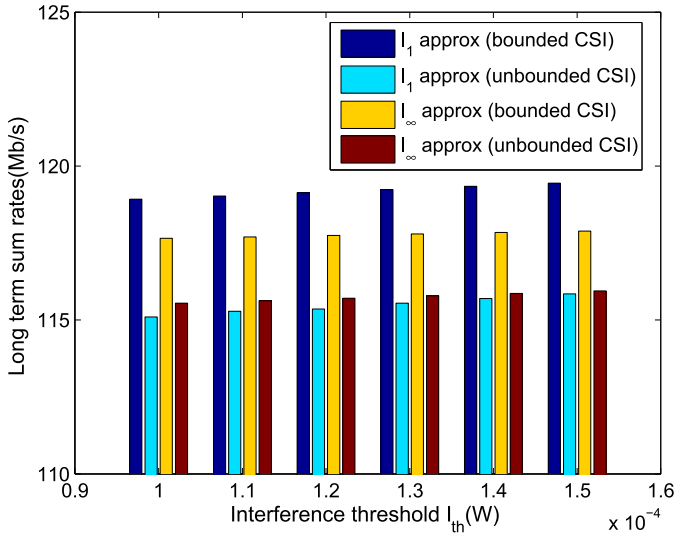

Fig. 7. Long term sum rates versus I_{th} when ε=0.3.

In order to further verify the system robustness, Fig. 8 shows the comparison of probabilistic audit when the bounded and unbounded cases are considered. Here, the real outage percentage (ROP) is captured by conducting 10^4 experiments for the statistic channel model. More specifically, Fig. 8(a) and Fig. 8(b) show the relationship between ROP and target outage threshold ε when the cases of bounded CSI and unbounded CSI are considered respectively. Both the black dot dash lines in the two subgraphs show that the target outage threshold ε are equal to the ROPs. The two subgraphs also show that the ROP of ℓ_1-approximation is smaller than that of the ℓ_∞-approximation when the same target outage threshold is used. These results indicate that ℓ_1-approximation is more conservative. Furthermore, Fig. 8(b) shows the results when ε is replaced with ε'. This simulates the case when the unbounded CSI is required to be converted to the bounded CSI of which the Bernstein approximation is used. Unlike the cases of unbounded CSI in Fig. 8(b), Fig. 8(a) shows that higher ROP can be achieved. Hence, the cases of unbounded CSI are more conservative than those of bounded CSI. Since all ROPs are smaller than the target value ε, a well-functioning D2D-V system can be guaranteed.

To illustrate the advantage of our proposed method in ROP, we have compared the performance index with the method developed in [18]. In [18], the system model is the same as the proposed method. However, the deterministic constraint can only be formulated for the CU's interference and the constraint cannot address the effect of channel uncertainty. Fig. 9 shows the comparison between the our four cases and the case with perfect CSI in [18] when the Doppler shift effect caused by speed is not considered. To achieve such a simulation environment, all vehicles's velocities are set to zero. Since the ROP in the four cases obtained by our proposed method are smaller than the perfect CSI case [18], this result indicates that our proposed power control schemes which are able to address channel uncertainty are more robust than the existing scheme [18]. The comparison result also shows that the case of ℓ_∞-approximation with

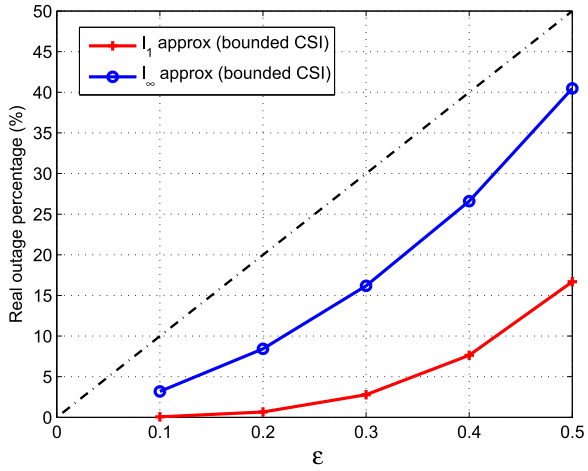

(a) Probabilistic audit in the case of bounded CSI.

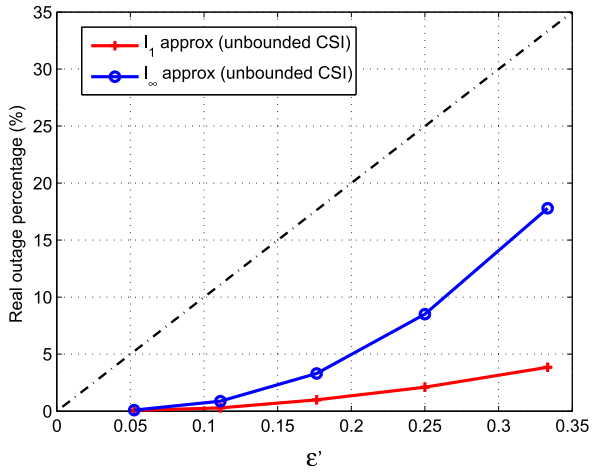

(b) Probabilistic audit in the case of unbounded CSI.

Fig. 8. Comparison of probabilistic audit in different cases.

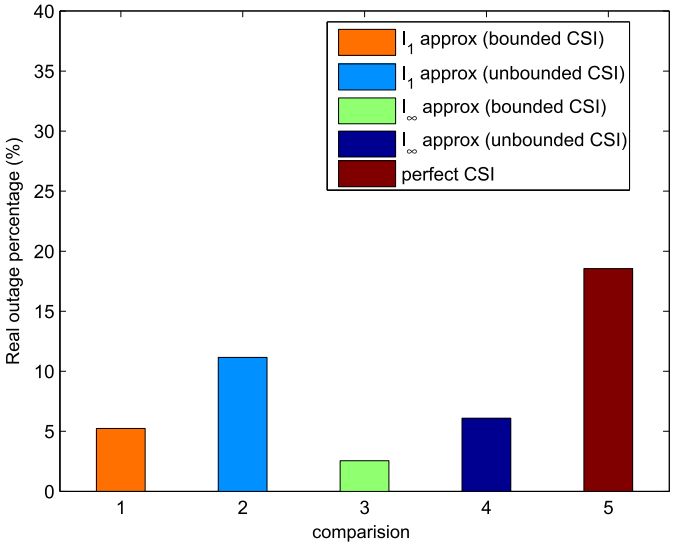

Fig. 9. The real outage probability without Doppler shifts.

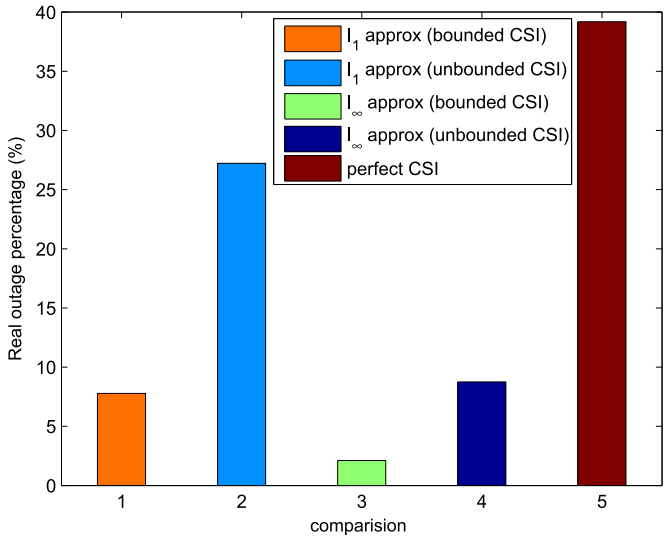

Fig. 10. The real outage probability with Doppler shifts.

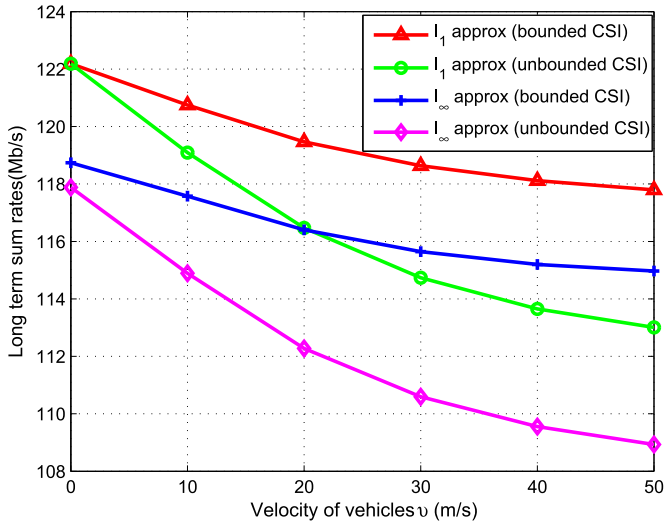

Fig. 11. Long term sum rates versus υ when $\varepsilon = 0.3$.

bounded CSI has the strongest robustness to resist channel fluctuations. Moreover, Fig. 10 shows the comparison between our proposed method and the existing method [18] when the Doppler shift effect is considered. All vehicle velocities are shown in Table IV. Compared with Fig. 9, Fig. 10 shows that higher ROP can be achieved in terms of all cases. The comparison result demonstrates the detrimental impact of Doppler shift exists on the D2D-V system.

Fig. 11 demonstrates the impacts to system performance when different vehicle speeds are simulated in a high mobility vehicular environment. In this simulation, all vehicle velocities are identical, and network topologies are the same. Hence, the cosine of the intersection angle between V2I links and velocity directions of vehicles is also the same. The Doppler shift effect of V2V links can be ignored since the relative velocity differences between the V2V links are zero. Thus, the impacts of system performance are mainly caused by the relative velocity

differences between the V2I links. The figure shows that the long term sum rates of D2D-V links decreases when the unified vehicle velocities increase from 0 to 50 m/s. The sum system capacity drops since the higher speed induces a larger Doppler shift, which increases the channel uncertainty of V2I links. The result shows that the sum system capacity with unbounded CSI decreases faster than the case with bounded CSI when the vehicle velocities increase, when the downtrend of ℓ_1-approximation is the same as the ℓ_∞-approximation. This phenomenon demonstrates that the cases with bounded CSI are more robust to the fluctuations of vehicle velocities than the cases with unbounded CSI.

Based on the simulation results, we can conclude that a sufficient margin should be set in a well-designed D2D-V system in order to resist interference and channel fluctuation since the aggregated random fluctuant interference signals are likely to cause CU's connectivity disruptions. In particular, higher CU's interference threshold value not only improves the sum rates of all D2D-V links, but also enhances the system robustness. Besides, if there is more comprehensive prior knowledge of CSI, the power control scheme with unbounded CSI should be used to design the optimal strategy because more prior knowledge leads to more accurate approximation. And the ℓ_∞-approximation algorithm is more conservative than ℓ_1-approximation algorithm. Consequently, the ℓ_1-approximation algorithm is recommended to design the optimal strategy for the real environment.

VI. Conclusion

In this paper, we have proposed a novel optimization scheme to solve the power control problem with high channel uncertainty. In the power control problem, the original objective function and probability constraint are nonconvex and intractable. The proposed scheme adopted the SCA and Bernstein convex approximation method to pursue a convex optimization problem. In the proposed scheme, two tractable approximate constraints are reformulated to a separable structure and the efficient near-optimal solutions can be found more easily. To tackle these two forms of channel uncertainty, the distributed iterative algorithm is proposed by the dual decomposition theory for approximating the two separable structures where two cases with the bounded CSI and the unbounded CSI are integrated. Although the simulation results demonstrate that the vehicle velocities have unfavorable impacts on system performance, the proposed optimization scheme is robust to the mobile channel fluctuations. Therefore, the system performance is satisfactory when high channel uncertainties exist in a highly mobility vehicular environment.

Appendix A

Assuming that Z is an independent random variable which is in the complex Gauss distribution with $\mathcal{CN}(0,1)$, and Z can be expressed as a complex variable with a real part and a imaginary part as,

$$Z = X + Yi, \tag{39}$$

where X and Y are identically distributed in $\mathcal{N}(0, \frac{1}{2})$; X is independent to Y. To be specified, the probability density functions of X and Y are given as

$$\begin{cases} f_X(x) = \frac{1}{\sqrt{\pi}} \mathrm{e}^{-x^2}, & -\infty < x < +\infty, \\ f_Y(y) = \frac{1}{\sqrt{\pi}} \mathrm{e}^{-y^2}, & -\infty < y < +\infty. \end{cases} \tag{40}$$

As a result, the combined probability density distribution function of X and Y are formulated as

$$f_Z(x,y) = f_X(x) f_Y(y) = \frac{1}{\pi} \mathrm{e}^{-(x^2+y^2)}. \tag{41}$$

The modulus length of Z is given as

$$|Z| = \sqrt{X^2 + Y^2}. \tag{42}$$

When $z = 0$, the probability density functions of $|Z|$, $f_{|Z|}(z) = 0$. When $z > 0$, the probability distribution function $F_{|Z|}(z)$ can be obtained as,

$$F_{|Z|}(z) = \int_{-\infty}^{+\infty} \int_{-\infty}^{+\infty} f(x,y) dx dy \tag{43}$$

Supposing that $X = R\cos t, Y = R\sin t$ $(0 \le R \le |Z|)$, the probability distribution function $F_{|Z|}(z)$ can be rewritten as

$$F_{|Z|}(z) = \int_0^{2\pi} \int_0^{|Z|} \frac{1}{\pi} \mathrm{e}^{-R^2} d\theta dR = 1 - \mathrm{e}^{-z^2}, \tag{44}$$

$$f_{|Z|}(z) = F'_{|Z|}(z) = 2z\mathrm{e}^{-z^2}. \tag{45}$$

Since $\psi_0^n = |h_0^n|^2$, we assume that $\Phi = |Z|^2$ $(|Z| \ge 0)$, and the probability distribution function $F_\Phi(\psi)$ is expressed as

$$\begin{aligned} F_\Phi(\psi) &= F(\Phi \le \psi) = F(|Z|^2 \le \psi) \\ &= F(0 \le |Z| \le \sqrt{\psi}) = 2\int_0^{\sqrt{\psi}} z\mathrm{e}^{-z^2} dz. \end{aligned} \tag{46}$$

Therefore, the density function of ψ is

$$f(\psi) = F'(\Phi \le \psi) = \left[2\int_0^{\sqrt{\psi}} z\mathrm{e}^{-z^2} dz \right]' = \mathrm{e}^{-\psi}. \tag{47}$$

The proof is completed.

Appendix B

Assuming that X is an independent exponential random variable with respect to the parameter Υ, which is given as

$$X \sim E(\Upsilon). \tag{48}$$

To be specified, the probability density function of X is described as

$$f(x) = \begin{cases} \Upsilon \mathrm{e}^{-\Upsilon x}, & x > 0 \\ 0, & x \le 0 \end{cases} \tag{49}$$

Another random variable Y, is defined as

$$Y = aX, \tag{50}$$

where a is a constant. The distribution function, is defined as

$$F(Y \le y) = F(aX \le y) = \int_0^{\frac{y}{a}} \Upsilon \mathrm{e}^{-\Upsilon x} dx. \tag{51}$$

Therefore, the probability density function of y is given as

$$f(y) = F'(Y \le y) = \begin{cases} \frac{\Upsilon}{a} \mathrm{e}^{-\frac{\Upsilon y}{a}}, & y > 0 \\ 0, & y \le 0 \end{cases}. \tag{52}$$

Therefore, the following relationship is proved to be true,

$$Y \sim E\left(\frac{\Upsilon}{a}\right). \tag{53}$$

The proof is completed.

APPENDIX C

Suppose that the distributions of $\tilde{g}_{k0}$ have the bounded supports of $[0, 2L_{k0}\sqrt{1-\epsilon_{k0}^2}]$, where the probability density function of $\tilde{g}_{k0}$ with mean $\bar{g}_{k0} = L_{k0}\sqrt{1-\epsilon_{k0}^2}$ is given as

$$f_{\tilde{g}_{k0}}(x) = \frac{1}{\bar{g}_{k0}} \mathrm{e}^{-\frac{x}{\bar{g}_{k0}}}. \tag{54}$$

Hence, we obtain $\alpha_k = \beta_k = L_{k0}\sqrt{1-\epsilon_{k0}^2}$. Based on (14), $\xi_k \in [-1, 1]$ and $\xi_k \sim E(1)$. The probability density function of ξ_k is formulated as

$$f_{\xi_k}(x) = \mathrm{e}^{-(x+1)}, x \in [-1, 1]. \tag{55}$$

The expectation and variance of ξ_k are given by

$$\mathbb{E}\{\xi_k\} = \int_{-1}^{1} x f_{\xi_k}(x) dx = -\frac{2}{\mathrm{e}^2} \approx -0.271,$$

$$\mathbb{D}\{\xi_k\} = \int_{-1}^{1} x^2 f_{\xi_k}(x) dx = 1 - \frac{5}{\mathrm{e}^2} \approx 0.323.$$

Refer to the Table I of [19], the values of μ_k^+ and r_k are as

$$\begin{aligned} &\mathbb{E}\{\xi_k\} \approx -0.271 < \mu_k^+ = 0.5 < r_k = \frac{\sqrt{2}}{2}, \\ &\mathbb{D}\{\xi_k\} \approx 0.323 < r_k^2 = 0.5 < 1. \end{aligned} \tag{56}$$

When (57) is defined,

$$q_{\mu,r}(t) \triangleq \begin{cases} \ln\left(\frac{(1-\mu)^2 \mathrm{e}^{\frac{t(\mu-r^2)}{1-\mu}} + (r^2-\mu^2)\mathrm{e}^t}{1-2\mu+r^2}\right), \text{if } t \ge 0 \\ \ln\left(\frac{(1+\mu)^2 \mathrm{e}^{\frac{t(\mu+r^2)}{1+\mu}} + (r^2-\mu^2)\mathrm{e}^{-t}}{1+2\mu+r^2}\right), \text{otherwise} \end{cases} \tag{57}$$

the values of σ_k can be obtained by solving

$$\sigma_k = \min\left\{c \ge 0 : q_{\mu_k^+, r_k}(t) \le \mu_k^+ t + \frac{c^2}{2}t^2, \ \forall t\right\}. \tag{58}$$

Since $t \ge 0$, $q_{\mu_k^+, r_k}(t) = \ln(\frac{1}{2} + \frac{1}{2}\mathrm{e}^t)$, when $\mu_k^+ = 0.5$ and $r_k = \frac{\sqrt{2}}{2}$.

Let

$$g(t) = \frac{1}{2}t + \frac{c^2}{2}t^2, \ t \ge 0,$$

$$f(t) = g(t) - q_{\mu,r}(t) = \frac{1}{2}t + \frac{c^2}{2}t^2 - \ln\left(\frac{1}{2} + \frac{1}{2}\mathrm{e}^t\right), \ t \ge 0. \tag{59}$$

When $t = 0$, $f(0) = 0$, $f'(0) = 0$, the function image of $g(t)$ is tangent to $q_{\mu,r}(t)$ at $t = 0$. $f'(t)$, the first derivative of $f(t)$, is expressed as

$$f'(t) = \frac{1}{2} + c^2 t - \frac{\mathrm{e}^t}{1+\mathrm{e}^t}. \tag{60}$$

To satisfy the conditions of (58), $f'(t) \ge 0, \forall t \ge 0$, (60) can be elaborated as,

$$f'(t) \ge 0 \Longrightarrow c^2 \ge \frac{(\mathrm{e}^t - 1)}{2(\mathrm{e}^t + 1)t}. \tag{61}$$

When $t > 0$ and $t \to 0$, $c^2 \ge \lim_{t\to 0} \frac{(\mathrm{e}^t-1)}{2(\mathrm{e}^t+1)t} = \frac{1}{4}$. Since $c \ge 0$, we can eventually obtain $\sigma_k = c_{\min} = \frac{1}{2}$.

The value of $c_{\min}$ can be verified through the function image generated by the Geometer's Sketchpad or MATLAB. Two adjacent values of $c_{\min}$'s can be selected as $c_1 = 0.4$ and $c_2 = 0.6$. Then, observe the position relation of two function images of $g(t)$ and $q_{\mu,r}(t)$ when c is equal to c_1 and c_2, respectively.

APPENDIX D

The lower bound approximation of the function $\log(1+x)$ is approximated as:

$$\log(1+x) \ge \alpha \log(x) + \beta, \ \ \forall x > 0, \tag{62}$$

where $\alpha > 0$ and β are the two coefficients which are required to be determined. Assume that the bound is tight at $x = x_0$, i.e. $\alpha \log(x_0) + \beta = \log(1 + x_0)$. Based on this tightness condition, the inequality (62) can be converted to

$$\left(\frac{x}{x_0}\right)^{\alpha} \ge \frac{1+x}{1+x_0}, \ \ \forall x > 0, \tag{63}$$

(63) indicates the following three facts:

1) Any α which meets (63) is a valid coefficient for the lower bound approximation;
2) The coefficient α must be less than one. Otherwise, $(\frac{x}{x_0})^{\alpha}$ is a concave function if $\alpha \ge 1$, and there exists some $x > 0$ such that (63) is not valid;
3) The function $y = \frac{1}{1+x_0}(1+x)$ is a tangent line for $y = (\frac{x}{x_0})^{\frac{x_0}{1+x_0}}$ at $x = x_0$.

Based on the three facts, it is concluded that $\alpha = \frac{x_0}{1+x_0}$ is the maximum value that satisfies (63). In this paper, we therefore choose the two coefficients as $\alpha = \frac{x_0}{1+x_0}$ and $\beta = \log(1+x_0) - \frac{x_0}{1+x_0}\log(x_0)$.

REFERENCES

[1] J. Mei, K. Zheng, L. Zhao, Y. Teng, and X. Wang, "A latency and reliability guaranteed resource allocation scheme for LTE V2V communication systems," *IEEE Trans. Wireless Commun.*, vol. 17, no. 6, pp. 3850–3860, Mar. 2018.

[2] X. Cao, L. Liu, Y. Cheng, L. X. Cai, and C. Sun, "On optimal device-to-device resource allocation for minimizing end-to-end delay in VANETs," *IEEE Trans. Veh. Technol.*, vol. 65, no. 10, pp. 7905–7916, Oct. 2016.

[3] W. Sun, E. G. Ström, F. Brännström, K. C. Sou, and Y. Sui, "Radio resource management for D2D-based V2V communication," *IEEE Trans. Veh. Technol.*, vol. 65, no. 8, pp. 6636–6650, Aug. 2016.

[4] X. Shen, X. Cheng, R. Zhang, B. Jiao, and Y. Yang, "Distributed congestion control approaches for the IEEE 802.11p vehicular networks," *IEEE Intell. Transp. Syst. Mag.*, vol. 5, no. 4, pp. 50–61, Oct. 2013.

[5] M. Fallgren and B. Timus, "Scenarios, requirements and KPIs for 5G mobile and wireless system," METIS, Stockholm, Sweden, ICT-317669-METIS/D1.1, 2013.
[6] A. Vinel, "3GPP LTE versus IEEE 802.11 p/WAVE: Which technology is able to support cooperative vehicular safety applications?" *IEEE Wireless Commun. Lett.*, vol. 1, no. 2, pp. 125–128, Apr. 2012.
[7] X. Cheng, L. Yang, and X. Shen, "D2D for intelligent transportation systems: A feasibility study," *IEEE Trans. Intell. Transp. Syst.*, vol. 16, no. 4, pp. 1784–1793, Aug. 2015.
[8] I. Stepanov, J. Haehner, C. Becker, J. Tian, and K. Rothermel, "A meta-model and framework for user mobility in mobile networks," in *Proc. Int. Conf. Netw.*, Sydney, NSW, Australia, Oct. 2003, pp. 231–238.
[9] M. Fiore and J. Härri, "The networking shape of vehicular mobility," in *Proc. 9th ACM Int. Symp. Mobile Ad Hoc Netw. Comput.*, 2008, pp. 261–272.
[10] J. Bunker and R. Troutbeck, "Prediction of minor stream delays at a limited priority freeway merge," *Transp. Res. B, Methodological*, vol. 37, no. 8, pp. 719–735, Sep. 2003.
[11] L. Vasconcelos, A. B. Silva, Á Seco, and J. Silva, "Estimating the parameters of Cowans M3 headway distribution for roundabout capacity analyses," *Baltic J. Road Bridge Eng.*, vol. 7, no. 4, pp. 261–268, 2012.
[12] D. Feng, L. Lu, Y. Yuan-Wu, G. Y. Li, G. Feng, and S. Li, "Device-to-device communications underlaying cellular networks," *IEEE Trans. Commun.*, vol. 61, no. 8, pp. 3541–3551, Aug. 2013.
[13] L. Liang, G. Y. Li, and W. Xu, "Resource allocation for D2D-enabled vehicular communications," *IEEE Trans. Commun.*, vol. 65, no. 7, pp. 3186–3197, Jul. 2017.
[14] H. Elsawy, E. Hossain, and M.-S. Alouini, "Analytical modeling of mode selection and power control for underlay D2D communication in cellular networks," *IEEE Trans. Commun.*, vol. 62, no. 11, pp. 4147–4161, Nov. 2014.
[15] M. Chiang, C. W. Tan, D. P. Palomar, D. O'Neill, and D. Julian, "Power control by geometric programming," *IEEE Trans. Wireless Commun.*, vol. 6, no. 7, pp. 2640–2650, Jul. 2007.
[16] M.-L. Ku, L.-C. Wang, and Y. T. Su, "Toward optimal multiuser antenna beamforming for hierarchical cognitive radio systems," *IEEE Trans. Commun.*, vol. 60, no. 10, pp. 2872–2885, Oct. 2012.
[17] F. Wang and W. Wang, "Sum rate optimization in interference channel of cognitive radio network," in *Proc. IEEE Int. Conf. Commun.*, 2010, pp. 1–5.
[18] Y. Ren, F. Liu, Z. Liu, C. Wang, and Y. Ji, "Power control in D2D-based vehicular communication networks," *IEEE Trans. Veh. Technol.*, vol. 64, no. 12, pp. 5547–5562, Dec. 2015.
[19] A. Ben-Tal and A. Nemirovski, "Selected topics in robust convex optimization," *Math. Program., Ser. B*, vol. 112, pp. 125–158, 2008.
[20] A. Nemirovski and A. Shapiro, "Convex approximations of chance constrained programs," *SIAM J. Optim.*, vol. 17, no. 4, pp. 969–996, 2006.
[21] N. Y. Soltani, S.-J. Kim, and G. B. Giannakis, "Chance-constrained optimization of OFDMA cognitive radio uplinks," *IEEE Trans. Wireless Commun.*, vol. 12, no. 3, pp. 1098–1107, Mar. 2013.
[22] S. Wang, W. Shi, and C. Wang, "Energy-efficient resource management in OFDM-based cognitive radio networks under channel uncertainty," *IEEE Trans. Commun.*, vol. 63, no. 9, pp. 3092–3102, Sep. 2015.
[23] Y. Zhang and S. Wang, "Resource allocation for cognitive radio-enabled femtocell networks with imperfect spectrum sensing and channel uncertainty," *IEEE Trans. Veh. Technol.*, vol. 65, no. 9, pp. 7719–7728, Sep. 2016.
[24] S. Xiao, X. Zhou, Y. Y. Wu, G. Y. Li, and W. Guo, "Robust resource allocation in full-duplex-enabled OFDMA femtocell networks," *IEEE Trans. Wireless Commun.*, vol. 16, no. 10, pp. 6382–6394, Oct. 2017.
[25] Q. Han, B. Yang, G. Miao, C. Chen, X. Wang, and X. Guan, "Backhaul-aware user association and resource allocation for energy-constrained hetnets," *IEEE Trans. Veh. Technol.*, vol. 66, no. 1, pp. 580–593, Jan. 2017.
[26] L. Liang, J. Kim, S. C. Jha, K. Sivanesan, and G. Y. Li, "Spectrum and power allocation for vehicular communications with delayed CSI feedback," *IEEE Wireless Commun. Lett.*, vol. 6, no. 4, pp. 458–461, Aug. 2017.
[27] T. Kim, D. J. Love, and B. Clerckx, "Does frequent low resolution feedback outperform infrequent high resolution feedback for multiple antenna beamforming systems?" *IEEE Trans. Signal Process.*, vol. 59, no. 4, pp. 1654–1669, Apr. 2011.
[28] R. Horst and H. Tuy, *Global Optimization: Deterministic Approaches*, 2nd ed. New York, NY, USA: Springer-Verlag, 1993.
[29] J. Papandriopoulos and J. Evans, "Low-complexity distributed algorithms for spectrum balancing in multi-user DSL networks," in *Proc. IEEE Int. Conf. Commun.*, 2006, pp. 3270–3275.
[30] S. Boyd and L. Vandenberghe, *Convex Optimization.* Cambridge, U.K.: Cambridge Univ. Press, 2004.
[31] R. D. Yates, "A framework for uplink power control in cellular radio systems," *IEEE J. Sel. Areas Commun.*, vol. 13, no. 7, pp. 1341–1347, Sep. 1995.
[32] S. K. Noh, P. j. Kim, and J. H. Yoon, "Doppler effect on V2I path loss and V2V channel models," in *Proc. Int. Conf. Inf. Commun. Technol. Convergence*, 2016, pp. 898–902.

Zhixin Liu received the B.S., M.S., and Ph.D. degrees in control theory and engineering from Yanshan University, Qinhuangdao, China, in 2000, 2003, and 2006, respectively. He is currently a Professor with the Department of Automation, Institute of Electrical Engineering, Yanshan University. He visited the University of Alberta, Edmonton, AB, Canada, in 2009. He is the author or coauthor of more than 80 papers in technical journals and conference proceedings. His current research interests include performance optimization and energy-efficient protocol design in wireless sensor networks, resource allocation in cognitive radio networks, and vehicular networks.

Yuan'ai Xie received the B.S. degree in automation from the North China University of Science and Technology, Tangshan, China, in 2016. He is currently working toward the Ph.D. degree in control science and engineering with Yanshan University, Qinhuangdao, China. His current research interests include wireless resource optimization, vehicular network, and D2D communication.

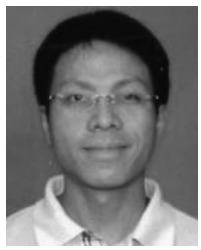

Kit Yan Chan received the Ph.D. degree in computing from London South Bank University, London, U.K., in 2006. He is currently a Senior Lecturer with the Department of Electrical and Computer Engineering, Curtin University, Bentley, WA, Australia. He was a Full Time Researcher with The Hong Kong Polytechnic University from 2004 to 2009 and with Curtin University from 2009 to 2013. His research interests include machine learning, pattern recognition, and algorithm design. He was the Guest Editor for the IEEE TRANSACTIONS INDUSTRIAL INFORMATICS, *Applied Soft Computing*, *Neurocomputing*, and *Engineering Applications of Artificial Intelligence*.

Kai Ma received the B.Eng. degree in automation and the Ph.D. degree in control science and engineering from Yanshan University, Qinhuangdao, China, in 2005 and 2011, respectively. In 2011, he joined Yanshan University. From 2013 to 2014, he was a Postdoctoral Research Fellow with Nanyang Technological University, Singapore. He is currently a Professor with the Department of Automation, School of Electrical Engineering, Yanshan University, Qinhuangdao, China. His current research interests include demand response in smart grid and resource allocation in communication networks.

Xinping Guan (F'18) received the B.S. degree in mathematics from Harbin Normal University, Harbin, China, in 1986, and the M.S. degree in applied mathematics and the Ph.D. degree in electrical engineering from the Harbin Institute of Technology, Harbin, China, in 1991 and 1999, respectively. He is currently a Professor with the Department of Automation, School of Electronic, Information, and Electrical Engineering, Shanghai Jiao Tong University, Shanghai, China. He is the author or coauthor of more than 200 papers in mathematical and technical journals. His current research interests include wireless sensor networks, congestion control of networks, robust control, and intelligent control for nonlinear systems.